Liquid Crystals
Publication details, including instructions for authors and subscription information:
http://www.informaworld.com/smpp/title~content=t713926090

Analysis of transient periodic textures in nematic polymers

Alejandro D. Rey[ab]; Morton M. Denn[a]
[a] Center for Advanced Materials, Lawrence Berkeley Laboratory and Department of Chemical Engineering, University of California, Berkeley, California, U.S.A. [b] Department of Chemical Engineering, McGill University, Montreal, Canada

To cite this Article Rey, Alejandro D. and Denn, Morton M.(1989) 'Analysis of transient periodic textures in nematic polymers', Liquid Crystals, 4: 4, 409 — 422
To link to this Article: DOI: 10.1080/02678298908035487
URL: http://dx.doi.org/10.1080/02678298908035487

LIQUID CRYSTALS, 1989, VOL. 4, NO. 4, 409–422

Analysis of transient periodic textures in nematic polymers

by ALEJANDRO D. REY† and MORTON M. DENN
Center for Advanced Materials, Lawrence Berkeley Laboratory and
Department of Chemical Engineering, University of California, Berkeley,
California 94720, U.S.A.

A numerical solution of the Leslie–Ericksen equations for nematic liquid crystals is obtained for in-plane rotation of a strong magnetic field. A transient periodic orientation develops as a result of in-plane director motion and the induced shear flow. At long times the in-plane director orientation results in steady *splay–bend inversion walls*. A linear stability analysis shows that the inversion walls are unstable to perturbations out of the plane for elastic coefficients characteristic of nematic polymers. Calculations of transmitted light intensity through crossed polarizers for the computed orientation development predict the evolution of a banded texture, as observed experimentally.

1. Introduction

Transient periodic textures are observed in nematic polymers during orientation in a magnetic field [1–5] and during relaxation following shear [6–10]. There is no conclusive analysis indicating a connection between these two phenomena, but they do exhibit the same apparent macroscopic response. We present a treatment here of the kinetics of periodic textures induced by magnetic orientation. It is possible that the understanding of this phenomenon will elucidate mechanisms for the banded textures during shear relaxation as well.

Nematic liquids have uniaxial symmetry described by a unit director **n** whose orientation is affected by the presence of bounding surfaces, electromagnetic fields, and flow fields. The liquid responds to orienting fields through curvature elasticity, characterized by three basic modes of deformation: splay, twist, and bend [11]. If a nematic liquid has a positive anisotropic diamagnetic susceptibility, a sufficiently high magnetic field will tend to co-align the director everywhere except in a small region near the bounding surfaces [11, 12]. A transient periodic response, giving rise to banded textures under polarized light, is common with nematic polymers when an oriented sample is subjected to a sufficiently strong field transverse to the initial uniform director orientation. This periodic response is due to strong back-flow effects (coupling between fluid flow and director reorientation), in which opposed rotating regions produce shear flows characterized by lower viscosities than those in pure rotation. This kinetic mechanism favors short wave lengths, but short wave lengths tend to increase the total elastic energy. The competing effects find an optimal balance, resulting in a fastest growing periodic mode [1].

In this work we use the Leslie–Ericksen continuum theory [11, 13] to describe the temporal evolution of the macroscopic orientation and velocity fields, neglecting fluctuations [14] but taking into account the nonlinearities at longer times and the formation of splay-bend inversion walls [11]. We show that the mechanism for the

† Present address: Department of Chemical Engineering, McGill University, Montreal, Canada H3A2A7.

0267–8292/89 $3.00

initial decay of the periodic structures is through an out-of-plane instability, which occurs when there is enough anisotropy in the elastic constants of the nematic polymer to induce a transition from a splay-bend wall to a twist wall.

2. Theory and balance equations

The free energy density of the elastic deformation, F, is given in the Leslie–Ericksen theory of nematic continua by

$$2F = K_{11}(\nabla \cdot \mathbf{n})^2 + K_{22}(\mathbf{n} \cdot \nabla \times \mathbf{n})^2 + K_{33}|\mathbf{n} \times \nabla \times \mathbf{n}|^2, \tag{1}$$

where K_{11}, K_{22} and K_{33} are the elastic constants for splay, twist, and bend, respectively. The kinematic variables are the velocity, $\mathbf{v}$, and the director, $\mathbf{n}$. These fields are coupled through the antisymmetric part of the stress tensor, hence flow induces orientation and reorientation induces flow. The fluid is treated as incompressible, with a density ϱ. The inertia of the director is neglected. The balance equations, using cartesian tensor notation, are

$$\varrho \dot{v}_i = F_i + t_{ji,j} \tag{2a}$$

and

$$0 = G_i + g_i + \pi_{ji,j}. \tag{2b}$$

The mechanical quantities are as follows: F_i, external body force per unit volume; G_i, external director body force per unit volume; t_{ji}, stress tensor; π_{ji}, intrinsic director surface stress tensor; g_i, intrinsic director body force. The constitutive equations for the stresses are as follows:

$$\begin{aligned} t_{ji} = {} & -p\delta_{ji} - \frac{\partial F}{\partial n_{k,j}} n_{k,i} + \alpha_1 n_k n_m A_{km} n_i n_j + \alpha_2 n_j N_i \\ & + \alpha_3 n_i N_j + \alpha_4 A_{ji} + \alpha_5 n_j n_k A_{ki} + \alpha_6 n_i n_k A_{kj}, \end{aligned} \tag{3a}$$

$$g_i = \gamma n_i - \beta_j n_{i,j} - \frac{\partial F}{\partial n_i} + \lambda_1 N_i + \lambda_2 A_{ij} n_j, \tag{3b}$$

$$\pi_{ji} = n_i \beta_j + \frac{\partial F}{\partial n_{i,j}}. \tag{3c}$$

The kinematical quantities are defined as follows:

$$A_{ik} = \tfrac{1}{2}(v_{i,k} + v_{k,i}), \tag{4a}$$

$$N_i = n_i + \tfrac{1}{2}(v_{i,k} - v_{k,i}) n_k. \tag{4b}$$

A_{ik} is the rate of deformation tensor and N_i is the angular velocity of the director relative to that of the fluid. The $\{\alpha_i\}$ are the six Leslie viscosities [13]. λ_1 and λ_2 are defined as follows:

$$\lambda_1 = \alpha_2 - \alpha_3, \tag{5a}$$

$$\lambda_2 = \alpha_5 - \alpha_6 = -(\alpha_2 + \alpha_3). \tag{5b}$$

The scalar functions p and γ, and the vector function $\boldsymbol{\beta}$, are required because of the constraints of incompressibility and director unit length. The equality in the expression for λ_2 is due to Parodi [13]. Parameter values for the synthetic polypeptide poly-benzylglutamate (PBG) reported by Taratuta *et al.* [15] are listed in the table; this is one of the best-characterized nematic polymers, and these values are used for

Physical constants for PLG.

Viscosities	
(Pa s)	
α_1†	−2·280
α_2	−3·480
α_3	−0·014
α_4†	0·287
α_5	3·233
α_6	−0·261
Elastic constants (Newtons) × 10^{12}	
K_{11}	4·1
K_{22}	0·36
K_{33}	4·7
Anisotropic diamagnetic susceptibility (SI units) × 10^6	
χ_a	8·8

† Estimated using Marrucci hard rod theory [16] with an order parameter $S = 0{\cdot}8$.

subsequent numerical computations. It is significant that $K_{11} \approx K_{33} \gg K_{22}$. Two assumptions based on Marrucci's hard rod theory [16] are needed to complete the table. The value of the anisotropic magnetic susceptibility for the optically-active isomer PBLG from Du Pre *et al.* [17] is included in the table and is used in the numerical calculations. The number of this section is concerned with obtaining the partial differential equations describing the transient periodic structures. The phenomenon is best represented in cartesian (x, y, z) coordinates; see figure 1. The initial state is one of uniform alignment in the z-direction with a director field

$$\mathbf{n}_0 = (0, 0, 1). \tag{6}$$

At time $t = 0$ a uniform magnetic field is imposed in the x-direction,

$$\mathbf{H} = (H, 0, 0). \tag{7}$$

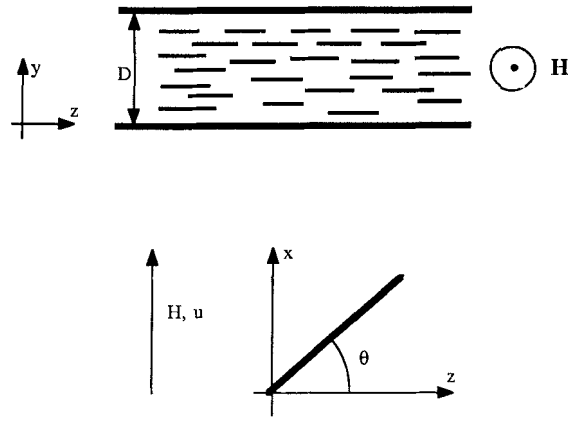

Figure 1. Schematic of the nematic cell at $t = 0$ and definition of coordinates. The applied field **H** is in the x direction. Cell surfaces are at $y = 0$ and D.

The x–z plane is assumed to be of infinite extent (i.e. D is much less than any characteristic dimension of the bounding surfaces of the cell).

Following Lonberg *et al.* [1] we first assume that the director is in the x–z plane,

$$\mathbf{n} = (\sin\theta, 0, \cos\theta) \tag{8}$$

where $\theta(x, y, z, t)$ describes the in-plane angle of the director relative to the initial orientation. The velocity field has a component only in the field direction,

$$\mathbf{v} = (u, 0, 0) \tag{9}$$

and, because of continuity, that component cannot depend on x. Since this is a reorientation-driven flow the pressure does not affect the linear momentum balance. In the presence of a magnetic field $\mathbf{H}$, the external director body force $\mathbf{G}$ is given by [18]

$$G_i = \chi_a H_i H_j n_j \tag{10}$$

where χ_a is the anisotropic diamagnetic susceptibility. With the above assumptions the director equation (2 *b*) becomes

$$\frac{h'}{2}\left(\frac{\partial\theta}{\partial z}\right)^2 + h\left(\frac{\partial^2\theta}{\partial z^2}\right) + K_{22}\left(\frac{\partial^2\theta}{\partial y^2}\right) - \lambda_1\left(\frac{\partial\theta}{\partial t}\right) - \frac{1}{2}(\lambda_2\cos\theta - \lambda_1)\frac{\partial u}{\partial z} + \tfrac{1}{2}\chi_a H^2 \sin 2\theta = 0. \tag{11}$$

Here

$$h(\theta) = K_{11}\sin^2\theta + K_{33}\cos^2\theta, \tag{12 a}$$

$$h'(\theta) = (K_{11} - K_{33})\sin 2\theta. \tag{12 b}$$

For $K_{11} = K_{33}$ we have $h = K_{11}$, $h' = 0$. The x-component of the momentum balance, equation (2.2 *a*), is

$$\varrho\frac{\partial u}{\partial t} = \eta_1\frac{\partial}{\partial z}\left(\frac{\partial\theta}{\partial t}\right) + \eta_2\left(\frac{\partial\theta}{\partial z}\right)\left(\frac{\partial\theta}{\partial t}\right) + \eta_3\left(\frac{\partial\theta}{\partial y}\right)\left(\frac{\partial u}{\partial y}\right) + \eta_4\left(\frac{\partial\theta}{\partial z}\right)\left(\frac{\partial\theta}{\partial t}\right) + \eta_5\left(\frac{\partial^2 u}{\partial z^2}\right) + \eta_6\left(\frac{\partial^2 u}{\partial y^2}\right), \tag{13}$$

where the angle-dependent combinations of viscosity coefficients $\{\eta_i\}$ are tabulated in Appendix A.

In the linear approximation of Lonberg *et al.* [1] the coefficients η_1, η_5, and η_6 are constants, while the terms containing the other $\{\eta_i\}$ in equation (13) and the quadratic term containing h' in equation (11) are neglected. This approximation will be valid in the limit $\theta \to 0$ (i.e. for short times). The resulting equations admit a solution in terms of Fourier components of the form

$$\theta(y, z, t) = \theta_0 \exp\left(\frac{\pi^2 s t}{D^2}\right)\cos\left(\frac{\pi z}{L}\right)\sin\left(\frac{\pi y}{D}\right),$$

$$u = \frac{-\alpha_2\pi s\theta_0}{L\left[\eta_a + \eta_c\dfrac{D^2}{L^2}\right]}\exp\left(\frac{\pi^2 s t}{D^2}\right)\sin\left(\frac{\pi z}{L}\right)\sin\left(\frac{\pi y}{D}\right), \tag{14 b}$$

θ_0 is the initial (infinitesimal) amplitude of the disturbance, and L is the Fourier wave length. The growth rate s is given by

$$s = \frac{\dfrac{\chi_a H^2 D^2}{\pi^2} - K_{22} - K_{33}\dfrac{D^2}{L^2}}{\lambda_1 - (\alpha_2^2)\left(\eta_c + \eta_a\left(\dfrac{L}{D}\right)^2\right)}, \tag{15}$$

with $2\eta_c = -\alpha_2 + \alpha_4 + \alpha_5$ and $2\eta_a = \alpha_4$. All modes grow in time as long as the field exceeds the critical value for a Freedericksz transition [11]. Since there is no interaction between modes in the linear theory, the wave length of the Fourier mode with the fastest growth rate will be observed. This mode will satisfy

$$\frac{ds}{dL} = 0, \tag{16}$$

which leads to a quadratic equation in $(D/L)^2$ in terms of the strength of the magnetic field, the elastic coefficients, and the rheological parameters.

In our nonlinear approach we assume that the periodic response at long times retains the dominant wave length defined by equation (16). Equations (11) and (13) are solved in dimensionless form with periodic boundary conditions at $z = 0$ and L and no slip ($u = 0$) and fixed anchoring ($\theta = 0$) conditions at $y = 0$ and D. The time and velocity scales of the transient are as follows, respectively:

$$\tau = \frac{\lambda_1}{\chi_a H^2}, \tag{17a}$$

$$U = \frac{\chi_a H^2 D}{\lambda_1}\left(\frac{L}{D}\right). \tag{17b}$$

For typical anisotropic susceptibilities of 10^{-6} SI units, the time scale for low molecular weight nematics is of the order of seconds, while for nematic polymers [19, 20, 21] it is of the order of minutes to hours.

All numerical solutions of the boundary value problem reported subsequently were obtained using the Galerkin finite element technique, with quadratic shape functions over ten elements in each coordinate (see, e.g., Fletcher [22]). Newton–Raphson iteration was used for solution of the non-linear system of algebraic equations. The time integration scheme was a first order Euler predictor–corrector method (see, e.g., Lapidus and Pinder [23]). Unless otherwise noted, the field strength was chosen to give $L/D = 3$, with D taken as 10^{-2} mm; this corresponds to a field of 15×10^{-3} tesla for the parameter values in the table. The linear solution with $\theta_0 = 10^{-2}$ radians was used to define conditions at $t = 0$. Parameter values are given in the table.

3. Numerical solutions

The maximum angle of distortion as a function of time is shown as the solid line in figure 2, with the linear theory given by equation (14*a*) as the dashed line. The maximum angle in our coordinate system occurs at $y/D = 0{\cdot}5$, $z/L = 0$. The linear solution is a good approximation for about the first 1·5 hours for the parameters characteristic of PBG, after which the exact solution tends to saturation at a new steady state value. The small difference in the initial growth rate is a result of the numerical discretization, and was found to decrease with refinement of the time integration step size. The maximum (centre plane) dimensionless velocity as a function of time is shown in figure 3. Again, the linear solution is a good approximation until about $t = 1{\cdot}5$ hours, after which the exact solution decays to zero as the director approaches the steady state value and the driving force for flow vanishes. The director orientation as a function of dimensionless position over half a wave length is shown in figure 4 at the midplane ($y/D = 0{\cdot}5$) and 40 and 80 per cent of the distance to the bounding plane. The parameter is the dimensionless time. The periodic distortions

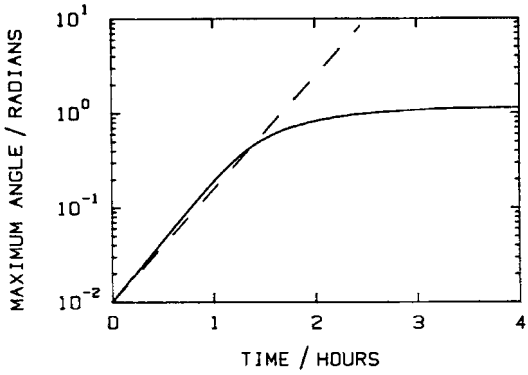

Figure 2. Computed maximum director angle as a function of time, $L/D = 3$. The dashed line is the linear solution (equation (14 *a*)).

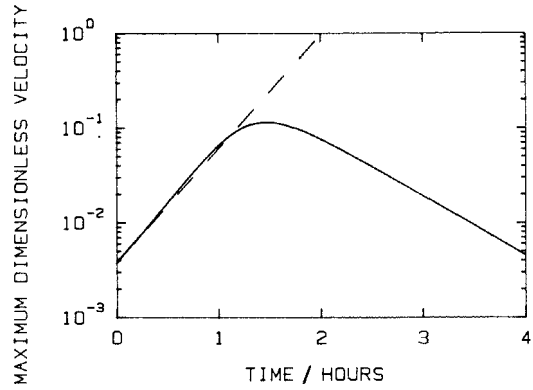

Figure 3. Computed maximum dimensionless velocity as a function of time, $L/D = 3$. The dashed line is the linear solution (Equation (14 *c*)).

involve large counter rotations at the edges of the cell, with the largest deformations at the midplane. The corresponding velocity profiles are shown in figures 5. (There is backflow in the right half of the cell to maintain continuity.) The strength of the magnetic field determines the time scale of the response and the magnitudes of the deformation and velocity fields. Time and velocity scale with H^2. The maximum steady state angle as a function of L/D is shown in figure 6. The effect here is a weak one, since there are two competing factors. Larger fields favor larger deformations, but shorter wave lengths favor smaller deformations. The transition region sharpens relative to L with decreasing field strength (corresponding to increasing L/D). The steady state center plane director profile is shown in figure 7 for $L/D = 30$, corresponding to $H = 9 \times 10^{-3}$ tesla for the parameters used here. This profile is of the form of a splay-bend wall; for $D \to \infty$ (i.e. in the absence of bounding planes) and $K_{11} = K_{33} = K$, a splay-bend wall is described by the equation [24]

$$\theta(z) = \tan^{-1}\exp\left[\pm z\sqrt{\left(\frac{\chi_a H^2}{K}\right)}\right]. \tag{18}$$

It is useful in what follows to note that equation (18) is closely approximated by a straight line in the interval $-d/2 \leqslant z \leqslant d/2$, and $\theta = \pm\pi/2$ otherwise, with d

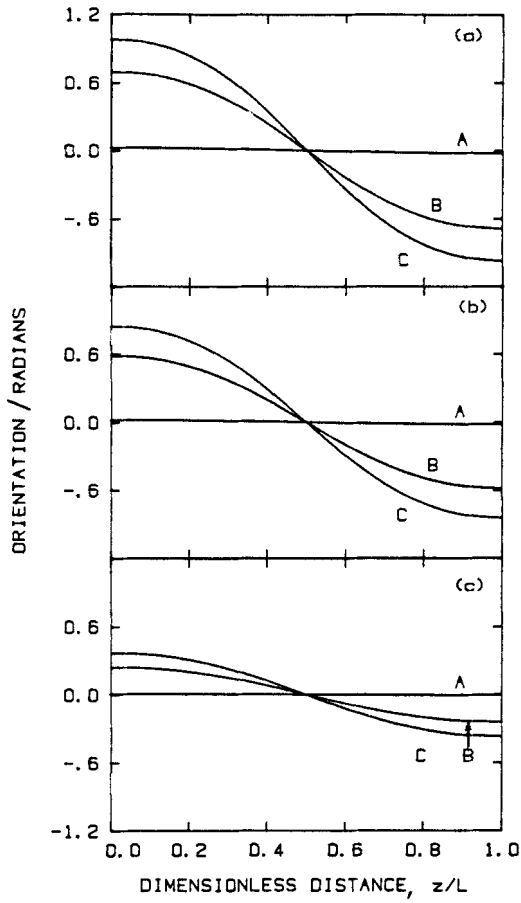

Figure 4. Director orientation profiles, $L/D = 3$. Curve A, $\chi_a H^2 t/\lambda_1 = 0{\cdot}51$; B, 2·88; C, 4·04. (*a*) $y/D = 0{\cdot}5$; (*b*) $y/D = 0{\cdot}7$; (*c*) $y/D = 0{\cdot}9$.

given by

$$d = \frac{1}{H}\sqrt{\left(\frac{K}{\chi_a}\right)}. \tag{19}$$

For finite D the structure is the same, with the wall thickness d scaling as H^{-1}, but the maximum angle is less than $\pi/2$.

It is important to note that the steady-state in-plane solutions computed here will lead to permanent banded textures, in contrast to the experimental observations cited in the introduction. We show in the next section that splay-bend walls are unstable to out-of-plane perturbations for values of the elastic coefficients reported for polymers, and the banded texture can not persist. This is consistent with the observation [24] that splay-bend walls have a larger surface tension than twist walls.

4. Linear stability analysis of splay-bend walls

To a first approximation, we can neglect the cell surface effects on the director and consider only the splay-bend deformations, neglecting the twist deformation close to the bounding surfaces. $\theta(z)$ is used to denote the steady-state solution. We consider

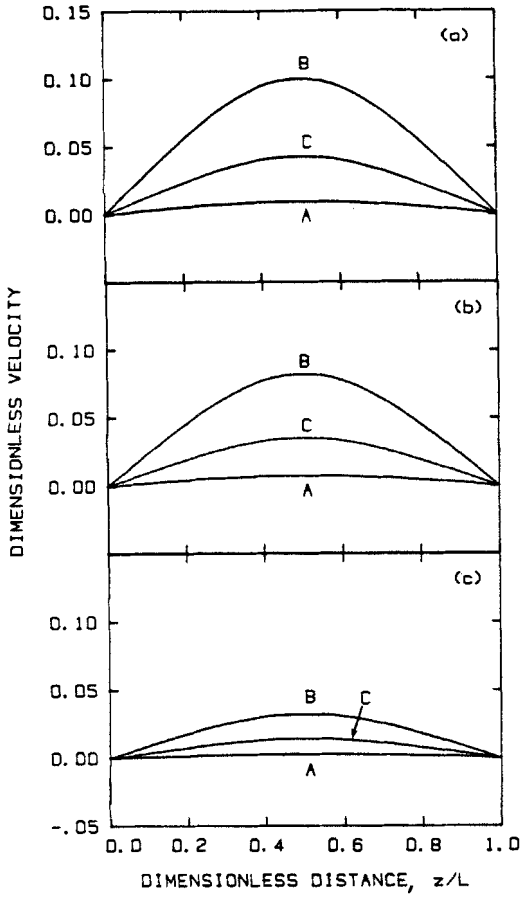

Figure 5. Dimensionless velocity profile, $L/D = 3$. Curve A, $\chi_a H^2 t/\lambda_1 = 0{\cdot}51$; B, 2·88; C, 4·04. (*a*) $y/D = 0{\cdot}5$; (*b*) $y/D = 0{\cdot}7$; (*c*) $y/D = 0{\cdot}9$.

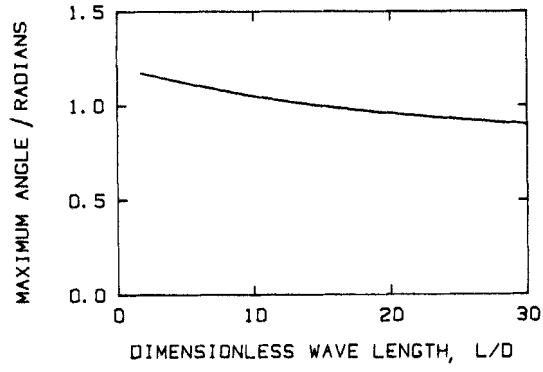

Figure 6. Effect of wave length ratio (equivalent to field strength) on the steady state maximum director angle.

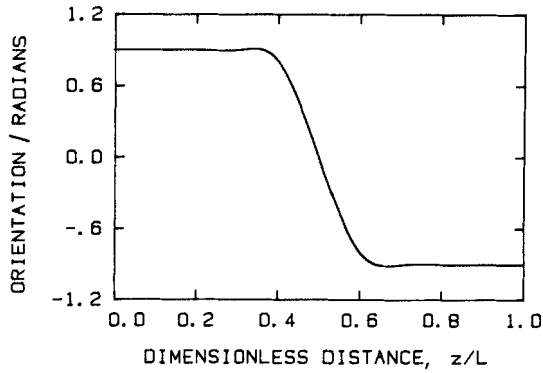

Figure 7. Steady state director orientation at the centre plane ($y/D = 0{\cdot}5$), $L/D = 30$.

small in- and out-of-plane perturbations $\psi(z, t)$ and $\xi(z, t)$, respectively, resulting in a director field given by

$$n_x = \sin\theta + \psi\cos\theta, \tag{20a}$$

$$n_y = \xi, \tag{20b}$$

$$n_z = \cos\theta - \psi\sin\theta. \tag{20c}$$

We neglect terms of order ψ^2 and ξ^2, in which case the director retains a unit magnitude. Substituting this director field into equation (2*b*) and retaining only linear terms in the perturbation, the evolution equation for the y (twist) component $\xi(z, t)$ becomes

$$\lambda_1 \frac{\partial \xi}{\partial t} = A(\theta)\,\xi + B(\theta)\,\xi_z + C(\theta)\,\xi_{zz} \tag{21}$$

where

$$A(\theta) = (3(K_{33} - K_{22})\cos^2\theta + K_{11} + K_{22} - K_{33})\theta_z^2 + (K_{11}\tan\theta + (K_{33} - K_{22})\sin\theta\cos\theta)\theta_{zz}, \tag{22a}$$

$$B(\theta) = (K_{22} - K_{33})\sin 2\theta, \tag{22b}$$

$$C(\theta) = (K_{33} - K_{22})\cos^2\theta - K_{22}. \tag{22c}$$

The boundary conditions are $\xi \to 0$ as $z \to \pm\infty$.

Equation (21) is parabolic with position dependent coefficients and must have solutions of the form

$$\xi(z, t) = \exp(\sigma t)\,\phi(z). \tag{23}$$

It is convenient to scale the length by the thickness of the splay-bend wall, d, given by equation (19). In that case the evolution equation (21) becomes

$$0 = [Ad^2 - \sigma\tilde{\lambda}_1]\phi + [Bd]\frac{d\phi}{d\zeta} + C\frac{d^2\phi}{d\zeta^2}, \tag{24}$$

where $\tilde{\lambda}_1 = \lambda_1 d$ and $\zeta = z/d$. This is an eigenvalue problem for the growth rate σ. Steady solutions given by equation (18) will be unstable to out-of-plane solutions if any eigenvalue is positive. Marginal stability is defined by $\sigma = 0$.

We use the linear approximation to the steady-state wall profile for convenience,

$$\theta(\zeta) = \frac{\pi}{2}(1 - 2\zeta) \tag{25}$$

in which case the boundary condition at infinity is replaced by

$$\phi = 0 \quad \text{at} \quad \zeta = 0, 1. \tag{26}$$

(Note that the origin has been moved to the edge of the wall for convenience.) The dominant eigenvalue is then obtained exactly. The first eigenfunction to equation (24) is readily shown to be

$$\phi = \sin(\pi\zeta). \tag{27}$$

The condition $\sigma \geqslant 0$ then follows immediately from equation (24) as

$$K_{22} \leqslant \frac{K_{11} + K_{33}}{2}, \tag{28}$$

which indicates that the wall is absolutely unstable to arbitrarily small symmetric perturbations unless the twist is at least equal to the average bend and splay elastic constants. K_{22} is found to be much less than K_{11} or K_{33} for nematic polymers.

Higher harmonics are not eigenfunctions, but a spectral method [25, 26] can be used to obtain approximations to the eigenvalues and eigenfunctions. Details are given by Rey [27]. The eigenvalues are real and ordered. The second and third eigenvalues at $\sigma = 0$ lead to critical conditions $K_{22} \leqslant (2K_{11} - 3K_{33})/(n^2 + 1)$ for $n = 2$ and 3, respectively, and these are clearly dominated by equation (28).

The linear approximation for ϕ is not necessary, but it simplifies the analysis greatly. Sufficient conditions for stability to infinitesimal perturbations can also be obtained analytically, and these do not require the linear approximation (though the analysis is again simplified) [27].

The linear theory can only account for initial growth of the out-of-plane perturbation, which will develop into a twist wall as shown in figure (8). The final stage in the defect-controlled dynamics is likely to be the rupture of the twist wall through the development of a pair of disclination lines [2].

5. Dynamics of banded textures

The experimental observations of the periodic response of nematic polymers by optical microscopy [1–3, 5] during magnetic instabilities result in the presence of

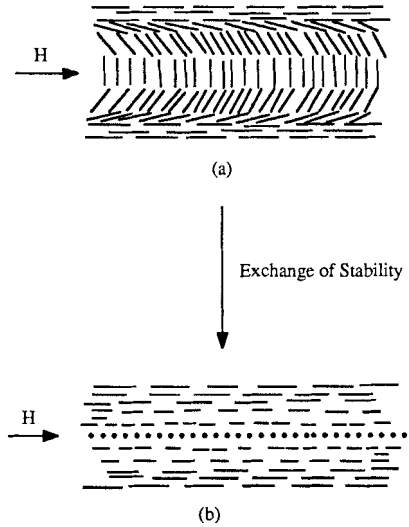

Figure 8. Schematic of wall transformation: (*a*) Splay-bend wall; (*b*) Twist wall.

transient banded textures. The bands consist of alternating dark and light parallel regions in the direction of the applied magnetic field. The evolution of the response can be followed with optical microscopy by continuously digitizing the recording camera output, as done by McClymer and Labes [28]. A qualitative comparison of our numerical calculations with the experimental observations of the dynamic banded textures can be effected by calculating the intensity of transmitted light.

Nematic polymers are optically uniaxial materials that divide a ray of linearly polarized light into an ordinary and an extraordinary beam of light (barring the exceptional case in which the light beam is perfectly aligned with the optic axis). As the light ray traverses the sample, a phase difference between these two beams occurs due to the difference in refractive indices. By placing the birefringent cell between a polarizer and an analyser, interference patterns due to the phase-lag between the two beams are obtained beyond the analyser. These interference patterns are the result of minimum or maximum light-intensity transmission. The differential phase difference $d\delta$ of a birefringent material within a path of length dy is given by [29]

$$d\delta(y) = \frac{2\pi}{\lambda}(n_e - n_0)\,dy, \tag{29}$$

n_0 and n_e are the refractive indices for the ordinary and extraordinary beams, respectively, and λ is the wave length of light. Here we have assumed that the difference between the refractive indices is small compared to their magnitudes, that the angle between the axis of indicence and the light rays within the cell is zero, and that the angle of the incident light beam with the optic axis is $\pi/2$ radians. The intensity $I(z, t)$ of transmitted light through the birefringent cell between crossed polarizers with the polarizer in the z-direction is [30]

$$I(z, t) = \int_0^D dy \left[E^2 \sin^2 2\theta(y, z, t) \sin^2\left(\frac{\delta}{2}\right)\right], \tag{30}$$

where E is the amplitude of the incident light and D is the cell thickness. The value of the integral when θ is aligned at 45° is $D/4$; we denote four times this value I_0 (i.e. $I_0 = DE^2 \sin^2(\delta^2/2)$), in which case the relative intensity of transmitted light $I_r(z/L, t)$ is

$$I_r(z/L, t) = \frac{I}{I_0} = \int_0^1 d(y/D)[\sin^2\theta \cos^2\theta]. \tag{31}$$

Figure 9 shows the computed evolution of the relative intensity of transmitted light I_r as a function of dimensionless distance z/L for a wave length $L/D = 3$. At early times (curve A) the intensity profile remains close to zero, but at longer times the middle region is isolated by regions of growing light intensity (curves B and C). As time goes on there is a sharpening of these regions, with the extinction region becoming narrower and the adjacent regions remaining of equal intensity but broader (curve D). The splay-bend walls cannot persist because of the out-of-plane instability, and they will give way to twist walls.

The evolution of the light intensity can be converted into a set of pictures by digitizing the profiles and linearly mapping the numbers onto a light scale. Figure 10 shows the appearance and evolution of the banded textures, in qualitative agreement with the experimental observations [1, 5] and measurements [28]. As expected, the early time behavior shows a homogeneously dark sample (curve A), which gives way to an incipient banded texture (curve B). At longer times there is a narrowing of the

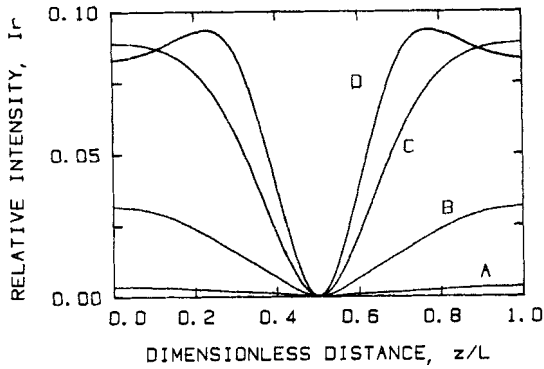

Figure 9. Computed relative intensity of transmitted light through crossed polarizers as a function of dimensionless distance, $L/D = 3$. Curve A, $t = 0{\cdot}88$ hours; B, 1·35; C, 2·38; D, 3·06. The polarizer is in the z-direction.

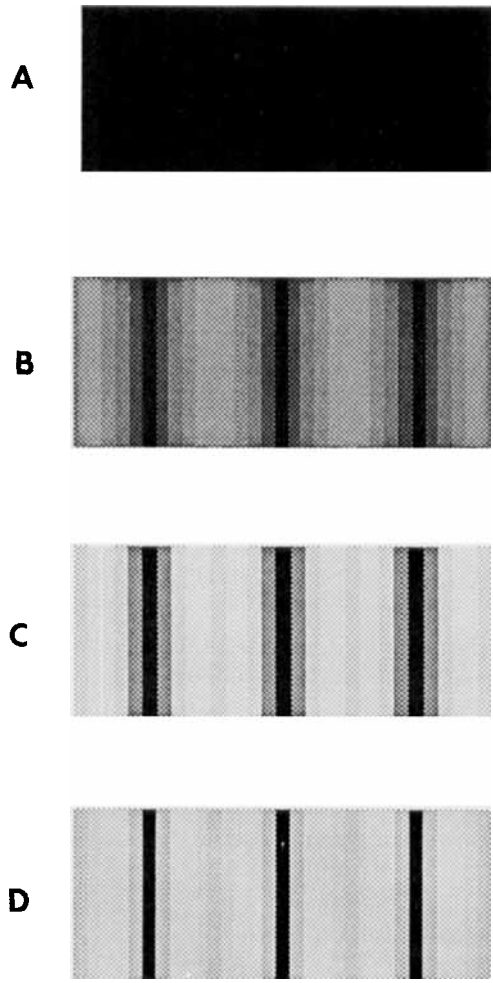

Figure 10. Digitized relative intensity of transmitted light as a function of dimensionless distance. The relative maximum intensity is white and the relative minimum is black. A to D correspond to the calculated values in figure 9.

dark regions, with a brightening of the lighter regions; these are the transient banded textures (curve C and D). At still longer times there is little variation in the distribution of the light intensity. These textures correspond to the splay-bend inversion walls (dark bands) separated by homogeneously aligned regions (light bands). As already shown, these walls are unstable to perturbations of the director out of the plane, and will result in twist walls that eventually pinch into disclination lines. A likely picture corresponding to the twist wall is one with thin dark lines separated by lighter regions. These visualizations are consistent with the detailed experimental observations of McClymer and Labes [28].

6. Conclusions

The Leslie–Ericksen theory of nematic continua is able to describe the development of the banded textures seen during the twist magnetic instability of nematic polymers. The linear approximation describes the short-time behaviour, but the non-linear terms are required to describe saturation of the director orientation and decay of the velocity field. The nonlinearities lead to an in-plane splay-bend wall at long times. Splay-bend inversion walls are unstable for most common nematic polymers because of anisotropy in the elastic constants, leading to growth of perturbations out of the plane. The perturbation probably evolves into a twist wall that decays into a pair of disclination lines that move towards the cell surface at later times, but this final stage can not be accounted for in the present analysis. The appearance and evolution of the banded structures predicted by calculating the intensity of transmitted light through crossed polarizers are consistent with the experimental results.

This work was supported by the Director, Office of Energy Research, Office of Basic Energy Sciences, Materials Science Division of the U.S. Department of Energy under Contract No DE-AC03-76SF 00098 and by a gift from E.I. Du Pont de Nemours & Co, Inc. We are grateful to C. R. Fincher for many useful discussions.

Appendix A

The coefficients η_i in equation (13) are

$$\eta_1 = \alpha_2 \cos^2\theta - \alpha_3 \sin^2\theta, \tag{A 1a}$$

$$\eta_2 = -(\alpha_2 + \alpha_3)\sin 2\theta, \tag{A 1b}$$

$$\eta_3 = \tfrac{1}{2}(\alpha_3 + \alpha_6)\sin 2\theta, \tag{A 1c}$$

$$\eta_4 = \tfrac{1}{2}\alpha_1(\sin 4\theta) + \tfrac{1}{2}(\alpha_2 + \alpha_3)\sin 2\theta, \tag{A 1d}$$

$$\eta_5 = \tfrac{1}{4}\alpha_1(\sin 2\theta)^2 + \tfrac{1}{2}\alpha_4 + \tfrac{1}{2}(\alpha_5 - \alpha_2)\cos^2\theta + \tfrac{1}{2}(\alpha_3 + \alpha_6)\sin^2\theta, \tag{A 1e}$$

$$\eta_6 = \tfrac{1}{2}\alpha_4 + \tfrac{1}{2}(\alpha_3 + \alpha_6)\sin^2\theta. \tag{A 1f}$$

The Parodi relation, equation (4*b*), has been used to simplify some equations.

References

[1] LONBERG, F., FRADEN, S., HURD, A. J., and MEYER, R. B., 1984, *Phys. Rev. Lett.*, **21**, 1903.
[2] FRADEN, S., HURD, A. J., MEYER, R. B., CAHOON, M., and CASPAR, D. L. D., 1985, *J. Phys., Paris*, **46**, C3–85.
[3] HURD, A. J., FRADEN, S., LONBERG, F., and MEYER, R. B., 1985, *J. Phys., Paris*, **46**, 905.
[4] LONBERG, F., and MEYER, R. B., 1985, *Phys. Rev. Lett.*, **55**, 718.

[5] FINCHER, C. R., 1986, *Macromolecules*, **19**, 2431.
[6] ASADA, T., 1985, *Polymeric Liquid Crystals*, edited by A. Blumstein (Plenum Press).
[7] DONALD, A. M., VINEY, C., and RITTER, A. P., 1986, *Liq. Crystals*, **1**, 287.
[8] VINEY, C., and WINDLE, A., 1986, *Polymer*, **27**, 1325.
[9] NAVARD, P., and ZACHARIADES, A. E., 1987, *J. Polym. Sci. Polym. Phys.*, **25**, 1089.
[10] MARRUCCI, G., GRIZZUTI, N., and BUONAURIO, A., 1987, *Molec. Crystals liq. Crystals*, **153**, 263.
[11] DE GENNES, P. G., 1975, *The Physics of Liquid Crystals* (Oxford University Press).
[12] CHANDRASEKHAR, S., 1977, *Liquid Crystals* (Cambridge University Press).
[13] LESLIE, F. M., 1979, *Adv. liq. Crystals*, **4**, 1.
[14] SAN MIGUEL, M., and SAGUES, F., 1987, *Phys. Rev.* A, **36**, 1883.
[15] TARATUTA, V., HURD, A., and MEYER, R., 1985, *Phys. Rev. Lett.*, **55**, 246.
[16] MARRUCCI, G., 1982, *Molec. Crystals liq. Crystals*, **72**, 153.
[17] DUPRE, D. B., 1982, *Polymer Liquid Crystals*, edited by A. Ciferri, W. R. Krigbaum, and R. B. Meyer (Academic Press).
[18] ERICKSEN, J. L., 1966, *Archs ration. Mech. Analysis*, **23**, 266.
[19] PLATE, N. A., and SHIBAEV, V. P., 1987, *Comb Shaped Polymers and Liquid Crystals* (Plenum Press).
[20] BLUMSTEIN, A. (editor), 1985, *Liquid Crystalline Order in Polymers* (Academic Press).
[21] ESNAULT, P., VOLINO, F., MARTINS, A. F., and BLUMSTEIN, A., 1987, *Molec. Crystals liq. Crystals*, **153**, 143.
[22] FLETCHER, C. A. J., 1984, *Computational Galerkin Methods* (Springer-Verlag).
[23] LAPIDUS, L., and PINDER, G., 1982, *Numerical Solution of Partial Differential Equations in Science and Engineering* (Wiley).
[24] HELFRICH, W., 1968, *Phys. Rev. Lett.*, **21**, 1518.
[25] DENN, M. M., 1975, *Stability of Reaction and Transport Processes* (Prentice Hall).
[26] CANUTO, C., HUSSAINI, M. Y., QUARTERANI, A., and ZANG, T. A., 1987, *Spectral Methods in Fluid Mechanics* (Springer-Verlag).
[27] REY, A. D., 1988, Ph.D. Thesis, Department of Chemical Engineering, University of California at Berkeley.
[28] MCCLYMER, J. P., and LABES, M. M., 1987, *Molec. Crystals liq. Crystals*, **144**, 275.
[29] BORN, M., and WOLF, E., 1980, *Principles of Optics* (Pergamon).
[30] SCHIEKEL, M. F., and FAHRENSCHAN, K., 1971, *Appl. Phys. Lett.*, **19**, 391.